Predicting the Effect of Hull Roughness on Ship Resistance using a Fully Turbulent Flow Channel and CFD

Roberto Ravenna[1,*], Ryan Ingham[2], Soonseok Song[3], Clifton Johnston[3], Claire De Marco Muscat-Fenech[4], Tahsin Tezdogan[1], Mehmet Atlar[1], Yigit Kemal Demirel[5]

[1]*Department of Naval Architecture, Ocean and Marine Engineering, University of Strathclyde, Glasgow, G1 0LZ, UK*
[2]*Department of Mechanical Engineering, Faculty of Engineering, Dalhousie University, Halifax, NS B3H 4R2, Canada*
[3]*Department of Naval Architecture & Ocean Engineering, College of Engineering, Inha University, Incheon, 22212, South Korea*
[4]*Department of Mechanical Engineering, Faculty of Engineering, University of Malta, MSD2080, Malta*
[5]*160 Bothwell Street, Glasgow, G2 7EA, UK*

Abstract: The effects of poor hull surface conditions on fuel consumption and emissions are well-known yet not thoroughly understood. Therefore, the present study investigates the effect of widely adopted fouling control coatings and mimicked biofouling on a full-scale representative ship, the KRISO Containership (KCS). Different surfaces were tested in the Fully turbulent Flow Channel (FTFC) of the University of Strathclyde (including a novel hard foul-release coating, commonly used antifouling, barrier resin, soft foul-release coatings, and sandpaper-like surfaces). Then, the corresponding roughness functions developed for the test surfaces were embedded in Computational Fluid Dynamics (CFD) simulations using the modified wall function approach. Interestingly, the numerical predictions on the KCS hull showed that the novel hard foul-release coating tested had better hydrodynamic performance than the smooth case (maximum 3.6% decrease in the effective power requirements). Eventually, the present study confirmed the practicality of the FTFC used in combination with CFD-based studies to predict the effects of hull roughness on ship resistance and powering.

Keywords: Fully Turbulent Flow Channel; Roughness Functions; Ship Resistance; Marine Coatings; Computational Fluid Dynamics.

1 INTRODUCTION

A ship's hull surface condition is crucial to its hydrodynamic performance (Schultz, 2007). Hence, choosing the right fouling control coating (FCC) and drydock strategies for a vessel can offer significant economic and environmental advantages. Theoretical and numerical methods based on the turbulent boundary layer similarity law scaling technique, which was proposed by Granville (Granville, 1978, 1958), can accurately predict the hull roughness effect on ship resistance, provided that the roughness function of the surface is known (Demirel, 2015).

The aim of this study is to obtain new roughness functions for commonly used marine coatings and biofouled hull conditions from Fully turbulent Flow Channel (FTFC) experiments and predict their effect on full-scale ship resistance and powering. Also, an important objective was to utilise the FTFC of the UoS, which is a more practical facility than a towing tank. Therefore, various types of FCCs were tested in the FTFC, including antifouling, soft foul-release, barrier resin coatings and the newly developed and patented hard foul-release coating (*FR02*) by Graphite Innovation & Technologies (GIT, 2021). Similarly, roughness functions were developed from FTFC tests for widely adopted sandpaper-like surfaces mimicking biofouled conditions (medium light slime and medium slime) as similarly done in towing tests (Schultz, 2004; Song et al., 2021c). Furthermore, the roughness functions developed for a sandpaper-like surface (*Sand 220*) from the FTFC experiments was compared with previous towing tank tests. Finally, the present study also aims to confirm the robustness of CFD-based methods to predict the effect of hull roughness on ship resistance and powering using FTFC-based roughness function models.

The remaining of the paper is structured as follows: Section 2 presents the methodology adopted, including the experimental setup, roughness functions development, CFD simulations, and experimental uncertainty analysis. Section 3 of the paper discusses the results of the current experimental and numerical investigation. Furthermore, the novel roughness functions of the test surfaces are presented and used to predict the variation of resistance coefficients and effective power requirements for the full-scale KRISO Container Ship (KCS) hull. Section 4 presents the conclusions of the study with some concluding remarks and recommendations for future studies.

2 METHODOLOGY

2.1. Approach

Figure 1 shows a schematic illustration of the experimental and numerical methodology adopted to investigate the roughness effects of marine coatings and hull roughness on the well-known KRISO Container Ship (KCS) ("KCS Geometry and Conditions," 2008). Drag characterisation of arbitrary rough surfaces on flat plates can be evaluated by the indirect method for pipes (Granville, 1987) that uses the pressure drop Δp which can be measured along the streamwise length of the coatings (i.e., the pressure drop method). The FTFC was used to determine the skin friction coefficients c_f, by measuring the pressure drop Δp on the test surfaces. Eventually, the roughness functions for the test surfaces were obtained (i.e., roughness functions, ΔU^+, roughness Reynolds numbers k^+, roughness length scale, k, etc.), and compared with literature, e.g., previous towing tests (Ravenna, 2019).

The modified wall function CFD simulations were adopted in the present study to predict the effect of the test surfaces on the full-scale KCS hull. The experimental roughness functions were embedded in CFD using the modified wall function approach to predict the effect of such surfaces on ship resistance and powering. The resistance coefficient results of the numerical predictions were then compared and validated across similar studies assessing the KCS resistance in smooth and rough conditions (Ravenna et al., 2022a; Song et al., 2020a; Yeginbayeva et al., 2020). Finally, the variations in effective power, ΔP_E due to each test surface were estimated to give an immediate understanding of the effects of marine coatings and hull roughness on ship resistance and powering. Comparison and validation of the ΔP_E values were conducted across the two numerical methods adopted and among similar studies (Schultz et al., 2011).

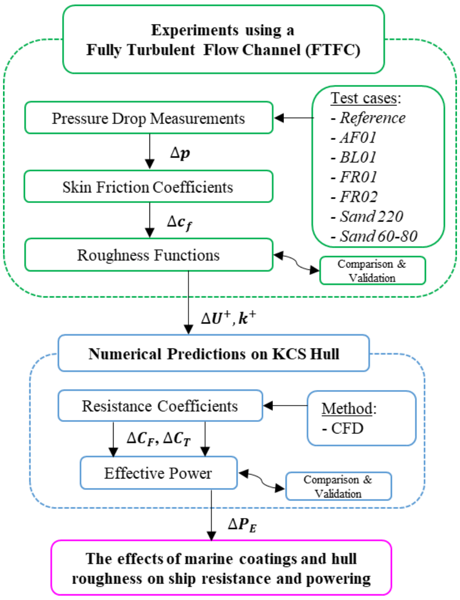

Figure 1: Schematic illustration of the methodology adopted.

2.2. Experimental Setup

2.2.1. Fully Turbulent Flow Channel

The University of Strathclyde's Fully Turbulent Flow Channel (FTFC), as shown in *Figure 2-a*, was designed to conduct a series of measurements for various types of fouling control coatings and rough surfaces in the freshly applied condition. Delivered to the UoS in 2019, the FTFC is a closed-circuit flow channel that can accommodate two opposing panels in its test section (*Figure 2-b*) located downstream of a single centrifugal pump. The results from the FTFC can be accurately analogised to the turbulent boundary layer formed on a ship's hull at cruising speed. In fact, the FTFC enables the measurement of much higher flow speeds that would not be otherwise achievable in a typical towing tank with flat friction test plates (Ravenna et al., 2019). *Table 1* summarises the main particulars of the FTFC upper limb section. For more information on the FTFC design, operation and calibration, the reader is advised to see (Marino et al., 2019).

(a) On-site picture of the FTFC.

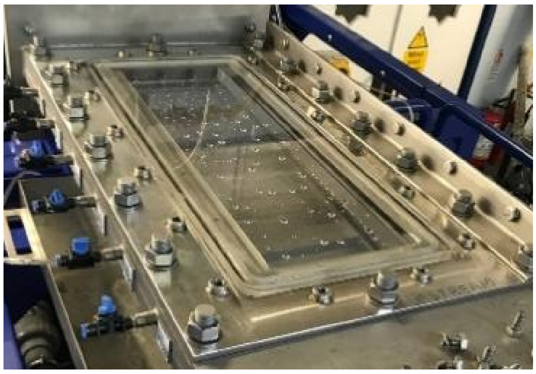

(b) Top view of the test section accommodating a couple of transparent smooth reference panels.

Figure 2: The Fully Turbulent Flow Channel (FTFC) of the University of Strathclyde.

Table 1: Main particulars of FTFC upper limb.

Name	Symbol	Unit	Value
Length (Tolerance)	l	mm	3000 (±0.05)
Height (Tolerance)	h	mm	22.5 (±0.05)
Beam (Tolerance)	b	mm	180 (±0.05)
Mean bulk velocity range	U_M	m/s	$1.5 - 13.5$
Flow rate	Q	l/s	$10 - 60$
Reynolds number	Re_M	-	$\approx 3.0 \cdot 10^5$
Material	-	-	Stainless steel (316L)
Centrifugal Pump power	P	kW	22

2.2.2. Test Panels Design and Preparation

In the present experimental campaign, four different types of FCCs were tested in the FTFC, including the newly developed hard foul-release coating (*FR02*) manufactured by GIT and marine coatings type that are commonly used in the shipping industry manufactured at Dalhousie University (DU), i.e., a self-polishing antifouling coating (*AF01*), a gelcoat barrier coating (*BL01*), and a soft foul-release coating (*FR01*). Furthermore, two sandpaper-like surfaces mimicking slime biofouling, i.e., *Sand 220* (medium light slime) and the coarser, *Sand 60-80* (medium slime) manufactured at the UoS were tested. The coated panels (*Figure 3*-a) were tested along with an uncoated "control surface" or the "reference" to represent a hydraulically smooth surface, *Figure 3-b*. *Table 2* describes the dimensions of the test panels, while a breakdown of the type of each marine coating applied and the method of application is provided in *Table 3*.

(a) Test panels coated with different fouling control coatings and sand grit.

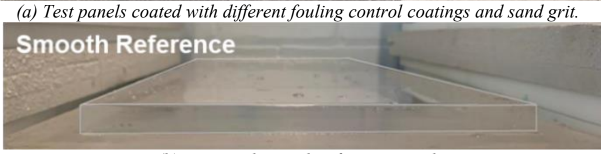

(b) Uncoated smooth reference panel.

Figure 3: Surfaces tested in the FTFC.

Table 2: Dimensions of the FTFC test panels.

Dimension	[mm]
Inner length	599
Inner breadth	218
Inner thickness	14
Outer length	662
Outer breadth	282
Outer thickness	16
Tolerance	0.1

Table 3: Overview of each test panel set.

Panel Set Name	Description (Prepared/Manufactured by)	Arithmetic mean roughness R_a [µm]
Reference	Smooth reference panel (UoS)	0.04
AF01	Self-Polishing antifouling coating (DU)	0.96
BL01	Gelcoat barrier coating (DU)	1.44
FR01	Soft foul-release coating (DU)	0.10
FR02	Hard foul-release coating (DU/GIT)	0.22
Sand 220	Aluminium oxide sand grit 220 (UoS)	294
Sand 60-80	Aluminium oxide sand grit 60-80 (UoS)	509

2.2.3. Pressure Drop Measurements

The UoS' FTFC facility is fitted with six pressure taps on the side opposite the laser window to measure the pressure drop (*Figure 4*). Pressure taps 2-5 were chosen for pressure drop measurements because this tap configuration showed the lowest uncertainty (1.48% - 1.23%) at the lowest and highest pump frequency, respectively (Marino et al., 2019). It is of note that the pressure taps are 120 mm apart from each other, and the pressure drop Δp is used in relation to the linear distance Δx to assess the skin friction of the surfaces, according to the following formulae from equations 1 to 4:

Skin friction coefficient: $$c_f = \frac{\tau_w}{\frac{1}{2}\rho U_M^2} \quad (1)$$

Wall shear stress: $$\tau_w = -\frac{D_h}{4}\frac{\Delta p}{\Delta x} \quad (2)$$

Hydraulic diameter: $$D_h = \frac{2\,hb}{h+b} \quad (3)$$

Reynolds number: $$Re_M = \frac{U_M\,h}{\nu} \quad (4)$$

where ρ, the water density, is specified based on the formulae provided by (ITTC, 2011a), including the correction for the temperature of the channel flow (i.e., around 18 °C), which is continuously recorded by the channel sensor.

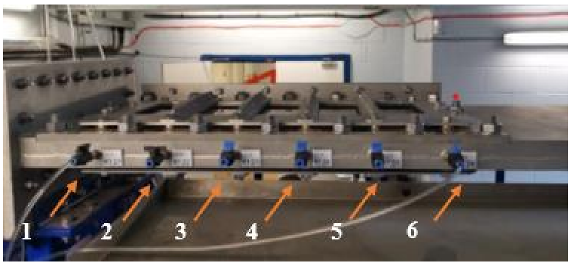

Figure 4: Pressure taps distribution numbered from 1 to 6 on test section of the FTFC.

2.3. Roughness Functions Determination

Roughness Function (or velocity loss function), ΔU^+, is further retardation of flow in the boundary layer over a rough surface due to the physical roughness of that surface, which manifests itself as additional drag relative to a smooth surface. Different surfaces are characterised by different roughness functions to be modelled experimentally (Granville, 1958). The roughness function, ΔU^+ is a function of the roughness Reynolds number, k^+, which is defined by Eq (5):

$$k^+ = \frac{kU_\tau}{\nu} \quad (5)$$

where, k is the roughness length scale of the surface, and U_τ is the friction velocity based on wall shear stress defined by Eq (6):

$$U_\tau = \sqrt{\tau_w/\rho} \quad (6)$$

where, τ_w is the wall shear stress.

For this study, the indirect method for fully developed pipe flow proposed by (Granville, 1987) is used to calculate the roughness function ΔU^+ and roughness Reynolds number k^+ for each coating as follows:

Roughness function: $$\Delta U^+ = \sqrt{\frac{2}{c_{f,s}}} - \sqrt{\frac{2}{c_{f,r}}} \quad (7)$$

Roughness Reynolds number: $$k^+ = \frac{1}{\sqrt{2}} Re_{M,r}\sqrt{c_{f,r}}\frac{k}{D_h} \quad (8)$$

where, $c_{f,s}$ and $c_{f,r}$ are the skin friction factors measured in the smooth and rough pipes, respectively, at the same value of $Re_M\sqrt{c_f}$. Furthermore, the hydraulic diameter, D_h of the channel was calculated by Eq (3).

It is of note that the selection of the roughness length scale, k, is critical to define a roughness function model, although k only affects the roughness Reynolds number, k^+. Therefore, k can be selected so that the roughness function models obtained are in agreement with the Nikuradse (Cebeci and Bradshaw, 1977; Nikuradse, 1933) or Colebrook type (Colebrook et al., 1939), provided that the observed behaviours are still deemed appropriate relative to each other. Accordingly, the k values were selected (*Table 6*) to get a good agreement between the present roughness functions and the Nikuradse type reference roughness function model.

2.4. CFD simulations

The present simulations were developed in the Star-CCM+ software package (Version 15.06.007-R8), adopting the Unsteady Reynolds Averaged Navier–Stokes (URANS)-based CFD with the modified wall-function model recently validated by Song et al. (Song et al., 2020c). The governing equations of the present CFD simulations are as in (Ferziger et al., 2020). Furthermore, the k-ω SST (Shear Stress Transport) turbulence model was used with a second-order convection scheme and the Volume of Fluid (VOF) model with Eulerian multiphase was used to simulate surface gravity waves on the interface between air and water. Finally, the free surface effects were modelled using High-Resolution Interface Capturing (HRIC). It is of note that the rationale behind the present CFD modelling choices can be found in (Ravenna et al., 2022b).

2.4.1. Geometry and Physical Settings

CFD simulations were carried out on the container ship KCS in full-scale, at a towing speed of 24 knots ($12.35\ m/s$), Froude number $Fn = 0.26$. The Reynolds number based on the ship speed and length was in the range of $Re_L = 2.72 \times 10^9$, which corresponds to the design speed of the full-scale KCS hull. *Table 4* presents the particulars of the full-scale and model KCS adapted from Kim et al. (Kim et al., 2001) and (Larsson et al., 2013).

Table 4: KRISO Container Ship (KCS) full-scale principal characteristics.

Parameters		
Scale factor	λ	1
Length between the perpendiculars	$L_{PP}\ (m)$	230
Length of waterline	$L_{WL}\ (m)$	232.5
Beam at waterline	$B_{WL}\ (m)$	32.2
Depth	$D\ (m)$	19.0
Design draft	$T\ (m)$	10.8
Wetted surface area w/o rudder	$WSA_{Total}\ (m^2)$	9424
Displacement	$\nabla\ (m^3)$	52030
Block coefficient	C_B	0.6505
Design speed	$V\ (kn;\ m/s)$	24; 12.35
Froude number	F_n	0.26
Reynolds number	Re	$2.72 \cdot 10^9$
Centre of gravity	$KG\ (m)$	7.28
Metacentric height	$GM\ (m)$	0.6

The computational domain of the present simulations is a virtual towing tank (*Figure 5*), and the size of the domain was chosen following the International Towing Tank Committee (ITTC) recommendations (ITTC, 2011b) and similar studies (Song et al., 2021a, 2021b, 2020b). For clean hull case, the smooth type of wall-function was used, whereas the rough type of wall-functions, containing the roughness functions of the test surfaces, were used for the rough surfaces of the hull. Finally, the model ship was free to sink and trim, as no constraints were given. *Figure 6* shows the volume mesh of the present CFD analysis. The built-in automated mesher of Star-CCM+ software was used to generate the trimmed hexahedral-dominant finite element mesh. Further near-wall mesh refinements were applied using prism layer meshes on the critical regions such as the free surface, the bulbous bow, and the stern. It is of note that for the present simulations, the wall y^+ values were kept between 30 and 300 and higher than k^+ values, as recommended by (Siemens, 2020), *Figure 7*. Furthermore, the average wall y^+ value is 190 and the number of cells is in the range of 1.4 million, and these values are in close agreement with (Dogrul et al., 2020). Finally, all the simulations used the same mesh regardless of the hull roughness scenarios.

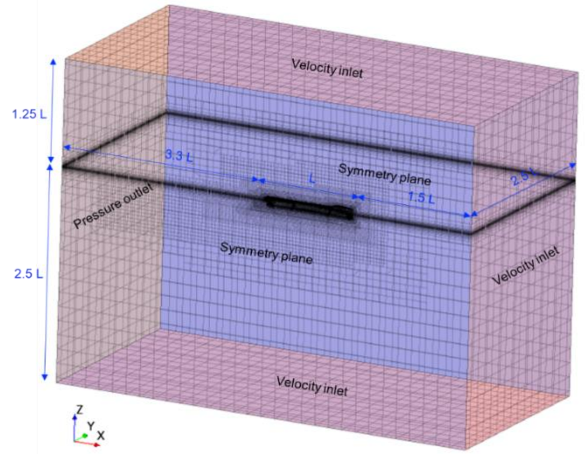

Figure 5: Computational domain and boundary conditions of the full-scale KCS simulations.

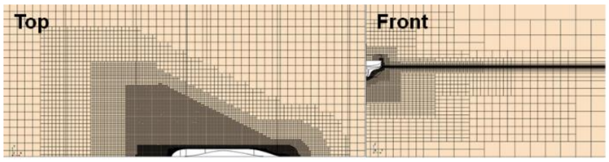

Figure 6: Volume mesh used for the KCS full-scale simulations.

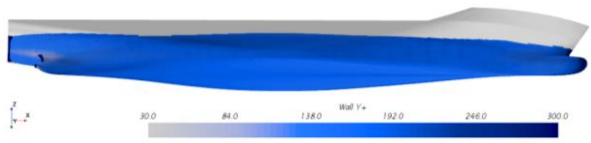

Figure 7: Non-dimensional wall distance y^+ of the full-scale KCS with homogenous hull roughness (*Sand 60-80*) towed at 24 knots ($Fn = 0.26$).

2.4.2. Modified Wall Function Approach

Eq (9) shows the roughness function model employed in the CFD software to represent the roughness conditions examined and obtain the variance in frictional resistance coefficients.

$$\Delta U^+ = \begin{cases} A & \rightarrow & k^+ < k^+_{smooth} \\ \frac{1}{\kappa} \ln C_s k^{+\,\sin\left[\frac{\pi}{2}\frac{\log(k^+/3)}{\log(25/3)}\right]} & \rightarrow & k^+_{smooth} \le k^+ < k^+_{rough} \\ \frac{1}{\kappa} \ln C_s k^+ & \rightarrow & k^+_{rough} \le k^+ \end{cases} \qquad (9)$$

(Cebeci and Bradshaw, 1977) recommended the following constants: $k^+_{smooth} = 2.25$, $k^+_{rough} = 90$, $A = 0$ and $C_s = 0.253$ for traditional Nikuradse roughness function and $C_s = 0.5$ for other roughness types. (Demirel et al., 2017) proposed $k^+_{smooth} = 3$, $k^+_{rough} = 15$ and $C_s = 0.26$ when fitting the roughness function proposed by (Schultz and Flack, 2007). In the results section of the present study (Section 3), different constants to develop the roughness function models for the surfaces tested will be introduced.

2.4.3. Verification and Validation

The verification procedure of the present CFD study was carried out to assess the spatial uncertainty of the simulations. Richardson's Grid Convergence Index (GCI) method (Richardson, 1911) was adopted as below. According to (Celik et al., 2008), the final expression for the fine-grid convergence index is defined as in equation (10):

$$GCI_{fine}^{21} = \frac{1.25 e_a^{21}}{r_{21}^{p_a} - 1} \tag{10}$$

where, e_a^{21} is the approximate relative error of the key variables, ϕ_k , obtained by equation (11), i.e., total resistance coefficient, C_T, as in equation (16):

$$e_a^{21} = \left|\frac{\phi_1 - \phi_2}{\phi_1}\right| \tag{11}$$

r_{21} is the refinement factor given by $r_{21} = \sqrt[3]{N_1/N_2}$, where N_1 and N_2 are the fine and medium cell numbers, respectively. Also, the apparent order of the method, p_a, is determined by solving equations (12) and (13) iteratively:

$$p_a = \frac{1}{ln(r_{21})} \left| ln\left|\frac{\varepsilon_{32}}{\varepsilon_{21}}\right| + q(p_a) \right| \tag{12}$$

$$q(p_a) = ln\left(\frac{r_{21}^{p_a} - s}{r_{32}^{p_a} - s}\right) \tag{13}$$

where $s = sign\left(\frac{\varepsilon_{32}}{\varepsilon_{21}}\right)$, $\varepsilon_{32} = \phi_3 - \phi_2$, $\varepsilon_{21} = \phi_2 - \phi_1$ and r_{32} is the refinement factor given by $r_{32} = \sqrt[3]{N_2/N_3}$, where N_3 is the coarse cell number.

The extrapolated value of the key variables is calculated by equation (14):

$$\phi_{ext}^{21} = \frac{r_{21}\phi_1 - \phi_2}{r_{21} - 1} \tag{14}$$

The extrapolated relative error, e_{ext}^{21}, is obtained by equation (15):

$$e_{ext}^{21} = \left|\frac{\phi_{ext}^{21} - \phi_1}{\phi_{ext}^{21}}\right| \tag{15}$$

Table 5: Parameters used for the discretisation error for the spatial convergence study, key variable: C_T.

	Full-scale KCS simulation
N_1	729,830
N_2	1,413,800
N_3	2,287,881
r_{21}	1.17
r_{32}	1.25
ϕ_1	$1.988 \cdot 10^{-3}$
ϕ_2	$1.996 \cdot 10^{-3}$
ϕ_3	$1.965 \cdot 10^{-3}$
ε_{32}	$-3.07 \cdot 10^{-5}$
ε_{21}	$7.10 \cdot 10^{-6}$
s	-1
e_a^{21}	0.36%
q	-0.33
p_a	7.04
ϕ_{ext}^{21}	$1.985 \cdot 10^{-3}$
e_{ext}^{21}	0.17%
GCI_{fine}^{21}	0.53%

Table 5 depicts the required parameters for the calculation of the spatial uncertainty of the simulation. A grid convergence index, GCI_{fine}^{21}, of 0.53% was estimated for the fine-grid simulations conducted in the smooth surface condition with the inlet speed of 24 kn ($R_n = 2.72 \cdot 10^9$), when using ten iterations every time step of 0.1 s. It is of note that the time step was selected following the recommendations of (ITTC, 2011b), for which $\Delta t = 0.005{\sim}0.01\, L_{WL}/V$, where L_{WL} is the ship length at waterline and V is the ship speed. In comparison to the simulations in (Song et al., 2020c), the number of cells in the present study is considerably less, guaranteeing a reduced computational cost without compromising the accuracy of the results. In fact, the estimated GCI value of 0.53% indicates the great accuracy of the present CFD resistance prediction. Furthermore, the resistance coefficient results of the smooth case agree with the results found in the literature. In fact, the discretisation errors for the spatial convergence study, GCI, found by (Dogrul et al., 2020; Song et al., 2020b) for the KCS model scale hull were 0.40% and 0.10%, respectively. Therefore, the present CFD simulations to predict the effect of hull roughness on ship resistance and powering are further validated.

2.5. Experimental Uncertainty Analysis

The uncertainties of the measurements in the FTFC tests were assessed following the ITTC-recommended procedures (ITTC, 2014). The standard errors for the coefficient of friction were calculated based on four to six replicate runs of the *FR01* panel at the minimum and maximum flow velocities, respectively. The precision uncertainty in the skin friction coefficient, c_f was calculated at a 95% confidence interval by multiplying the standard error by the two-tailed t values ($t = 3.182, 2.571$) for three to five degrees of freedom, according to (Coleman and Steele, 2012).

Notably, the accuracy of the differential pressure sensor is ±0.075%, and the accuracy of the magnetic flow meter was ±0.2%, according to the manufacturer's specifications. The total uncertainty in the roughness function (ΔU^+) was ±14.4% or 0.04 (whichever was larger) at the lowest Re_M ±6.5% or 0.04 (whichever was larger) at the highest Re_M. For comparison, the high Reynolds number turbulent flow facility at the US Naval Academy achieved a relatively similar level of uncertainty, with their skin friction data being ±1.2% at Re_M between $4.0 \cdot 10^4 - 3.0 \cdot 10^5$ (Schultz et al., 2015). The total bias limit and precision limit for the skin friction coefficients (c_f) were combined to give a total uncertainty of ±0.74% at the lowest Re_M and ±0.47% at the highest Re_M.

3 RESULTS AND DISCUSSION

3.1. Fully Turbulent Flow Channel Experiments

3.1.1. Roughness Function Models

As discussed in the methodology section (Section 2), provided that the roughness functions of the test surfaces are known, the CFD simulations can be used to predict the effect of hull roughness on ship resistance. Once the roughness functions have been calculated, they were directly compared with both Colebrook-type (Grigson,

1992) and Nikuradse-type (Cebeci and Bradshaw, 1977) roughness functions. Furthermore, the roughness functions of the sandpaper-like surfaces were compared for validation purposes with results obtained from other studies. In fact, previous flat plate towing tank experiments conducted for the same surface roughness (*Sand 220*) were used for comparison to the present results, *Figure 8*, (Ravenna, 2019). Finally, the new roughness functions have been developed using STAR-CCM+'s built-in features, as in Eq (9).

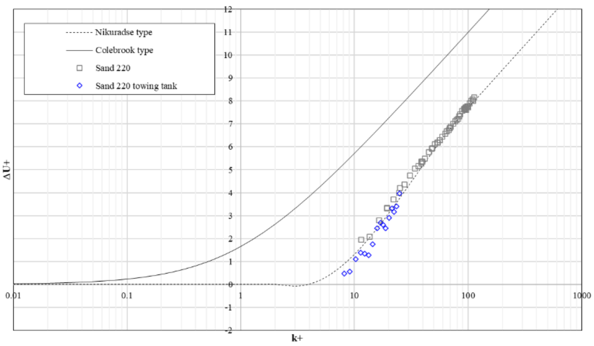

Figure 8: Experimental roughness function of the *Sand 220* surface developed from FTFC pressure drop measurements and from towing tank tests in (Ravenna, 2019).

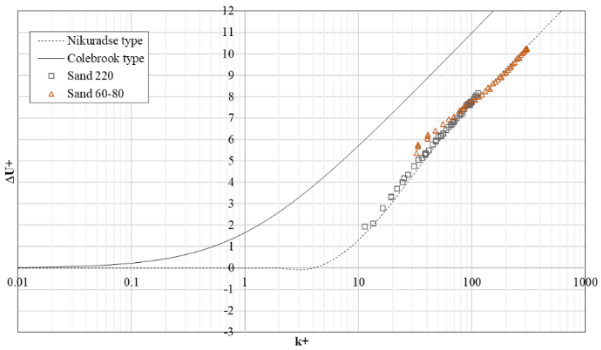

Figure 9: Experimental roughness functions of the sanded rough test surfaces (*Sand 220* and *Sand 60-80*) developed from FTFC pressure drop measurements.

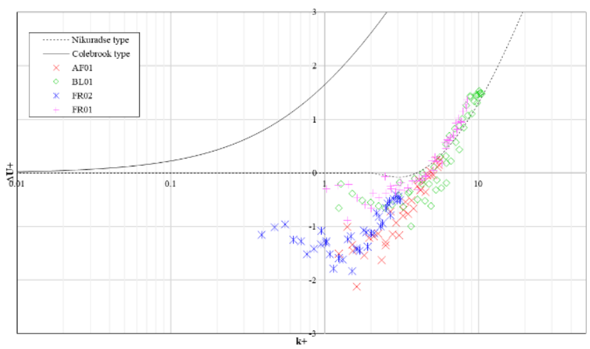

Figure 10: Experimental roughness functions of the sanded rough test surfaces (FCCs) developed from FTFC pressure drop measurements.

Figure 9, and *Figure 10* show the experimental roughness functions, ΔU^+, vs roughness Reynolds numbers, k^+ obtained from the FTFC pressure drop measurements following Granville's approach (Granville, 1987). It is of note that the experimental roughness functions of the FCCs tested were modelled by curve fitting to the roughness function model of Nikuradse. For completeness, in *Table 6* are presented the curve fitting coefficients used for all the surfaces tested, where E is the so-called turbulent wall function coefficient. In fact, in StarCCM+, the wall roughness is modelled by moving the logarithmic region of the boundary layer closer to the wall. To decrease roughness, E must be increased to incorporate this effect. Therefore, for the smoother and best performing surfaces (*AF01* and *FR02*) to which corresponded negative roughness function values, E was increased from the standard $E = 9$ to $E = 12$ and $E = 15$, respectively.

Table 6: Curve fitting coefficients of the roughness functions for the test surfaces.

Test Surface	Roughness length scale, k $[m]$	A	C_s	E	k_s^+	k_r^+
AF01	$9.598 \cdot 10^{-6}$	-1.5	0.2	12	1	15
BL01	$1.822 \cdot 10^{-5}$	-0.5	0.26	9	3	25
FR01	$1.544 \cdot 10^{-5}$	-0.5	0.2	15	3	25
FR02	$5.840 \cdot 10^{-6}$	-1.5	0.26	9	2	15
Sand 220	$1.532 \cdot 10^{-4}$	0	0.35	9	3	25
Sand 60-80	$3.530 \cdot 10^{-4}$	0	0.49	9	3	25

3.2. Numerical Prediction on full-scale KCS hull

3.2.1. *Ship Resistance Coefficients*

Numerical predictions were conducted on the benchmark KRISO containership hull at a towing speed of 24 knots ($Fn = 0.26$). The variance of resistance and powering requirements due to different test surfaces were calculated by incorporating the newly developed roughness functions into the Granville similarity law. The total resistance coefficient, C_T, is defined in equation (16) as a function of the total drag, R_T, the dynamic pressure, $1/2\ \rho V^2$, and the hull wetted surface area, S:

$$C_T = \frac{R_T}{1/2\ \rho\, S\, V^2} \tag{16}$$

where, V is the towing speed (i.e., the inlet velocity). It is well-known that the total ship resistance coefficient, C_T, can be decomposed into the frictional, C_F, and the residuary, C_R resistance coefficients, as given by Eq (17):

$$C_T = C_F + C_R \tag{17}$$

The variation of the frictional resistance coefficient ΔC_F is the difference between the rough, $C_{F,rough}$, and smooth, $C_{F,smooth}$, conditions at the same Froude number can be given by Eq (18):

$$\Delta C_F = C_{F_{rough}} - C_{F_{smooth}} \tag{18}$$

Hence, the variation of the frictional resistance due to the presence of roughness can also be expressed in percentage, as in equation (19):

$$\%\Delta C_F = \frac{C_{F_{rough}} - C_{F_{smooth}}}{C_{F_{smooth}}} \cdot 100 \tag{19}$$

The total resistance for the rough ship, $C_{T_{rough}}$, is determined by:

$$C_{T_{rough}} = C_{T_{smooth}} + \Delta C_T \tag{20}$$

where the total roughness allowance, ΔC_T is the variation in the total resistance coefficient between the rough,

$C_{T_{rough}}$, and smooth, $C_{T_{smooth}}$, conditions, and can be given by Eq (21):

$$\Delta C_T = C_{T_{rough}} - C_{T_{smooth}} \tag{21}$$

Figure 11 presents the resistance coefficients of the test cases obtained from the CFD simulations analysis compared to a hydrodynamically smooth ship hull. It is notable that the total resistance coefficient results are in good agreement and show similar trends to the frictional resistance coefficients Interestingly, the test cases *AF01* and *FR02* show a negative ΔC_T of 2.1% and 3.6%, respectively. As expected, the phenomena of reduced ΔC_T values are due to the negative roughness functions, ΔU^+ observed from the experimental measurements. On the other hand, the *BL01* and *FR01* cases lead to light ΔC_T increases (0.9% for *BL01* and 0.2% for *FR01*) compared to the total added resistance due to mimicked slime (27.7% for *Sand 220* and 36.1% *Sand 60-80* cases). Above all, it can be noted that the *FR02* is the best performing FCCs tested while the sanded surface, *Sand 60-80,* leads to a higher increase in the total resistance coefficients.

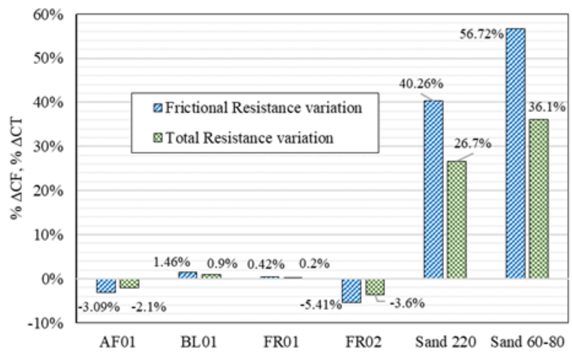

Figure 11: Frictional and total resistance coefficients variation in different hull roughness conditions.

Table 7, *Table 8* and *Figure 12* show the frictional and total resistance coefficients obtained for the test surfaces. It is also notable that the total resistance coefficient results are in good agreement and show similar trends to the frictional resistance coefficients. Furthermore, the results are reasonably in agreement with other studies found in the literature such as (Schultz, 2004; Yeginbayeva and Atlar, 2018).

Furthermore*,* the results are reasonably in agreement with other studies found in the literature such as (Schultz, 2004; Yeginbayeva and Atlar, 2018). In fact, (Schultz, 2004; Yeginbayeva and Atlar, 2018) found that a foul-release coating as applied measured an added frictional resistance $\%\Delta C_F$ equal to 2.6%, and for a 150 m flat plate at 12 knots coated with sand 60-80 calculated $\%\Delta C_F = 59\%$.

Table 7: Frictional resistance results (C_F) results on the full-scale KCS hull at 24 knots $(Fn = 0.26)$.

Test Surface	CFD simulations		
	C_F	ΔC_F	$\%\Delta C_F$
Reference	$1.309 \cdot 10^{-3}$	-	-
AF01	$1.268 \cdot 10^{-3}$	$-4.05 \cdot 10^{-5}$	-3.09%
BL01	$1.328 \cdot 10^{-3}$	$1.91 \cdot 10^{-5}$	1.46%
FR01	$1.314 \cdot 10^{-3}$	$5.44 \cdot 10^{-6}$	0.42%
FR02	$1.238 \cdot 10^{-3}$	$-7.08 \cdot 10^{-5}$	-5.41%
Sand 220	$1.835 \cdot 10^{-3}$	$5.27 \cdot 10^{-4}$	40.26%
Sand 60-80	$2.051 \cdot 10^{-3}$	$7.42 \cdot 10^{-4}$	56.72%

Table 8: Total resistance coefficients of the full-scale KCS at 24 knots $(Fn = 0.26)$.

Test Surface	CFD simulations		
	C_T	ΔC_T	$\%\Delta C_T$
Reference	$1.996 \cdot 10^{-3}$	-	-
AF01	$1.955 \cdot 10^{-3}$	$-4.096 \cdot 10^{-5}$	-2.05%
BL01	$2.015 \cdot 10^{-3}$	$1.860 \cdot 10^{-5}$	0.93%
FR01	$2.001 \cdot 10^{-3}$	$4.668 \cdot 10^{-6}$	0.23%
FR02	$1.925 \cdot 10^{-3}$	$-7.096 \cdot 10^{-5}$	-3.56%
Sand 220	$2.528 \cdot 10^{-3}$	$5.320 \cdot 10^{-4}$	26.66%
Sand 60-80	$2.717 \cdot 10^{-3}$	$7.210 \cdot 10^{-4}$	36.12%

3.2.2. *Ship Effective Power,* ΔP_E

The change in effective power, $\%\Delta P_E$ due to the different surfaces tested can be expressed by:

$$\%\Delta P_E = \frac{C_{T_{rough}} - C_{T_{smooth}}}{C_{T_{smooth}}} \cdot 100 = \frac{\Delta C_T}{C_{T_{smooth}}} \cdot 100 \tag{22}$$

similar to that used by (Tezdogan et al., 2015), where $C_{T_{smooth}}$ is the total resistance coefficient of the hull in smooth conditions obtained from the present CFD simulations. It is of note that $\%\Delta P_E$ is equal to $\%\Delta C_T$.

Table 9 shows the change in effective power, $\%\Delta P_E$ due to the different test cases obtained from the CFD simulations and Granville's approach. It is of note that the largest difference between coating types for powering requirements is an average of 4.75%, between *FR02* and *BL01.* As expected, if the coatings *AF01* and *FR02* were applied on the ship hull, they would lead to a reduction in effective power requirements. In fact, *AF01* guarantees a maximum decrease of power requirements of 2.31%, while *FR02* of 3.79%.

As expected, the phenomena are again due to the negative roughness functions, ΔU^+ observed from the experimental measurements to which correspond negatively ΔC_T values. On the other hand, the *BL01* and *FR01* cases lead to positive $\%\Delta P_E$, which translates into increases in effective power requirements of 0.93% for *BL01* and 0.23% for *FR01.* On the other hand, the total added effective power due to mimicked slime is 26.66% for *Sand 220* and 36.12% *Sand 60-80* cases. Above all, the *FR02* is the best performing FCCs tested while the sanded surface, *Sand 60-80,* would lead to a higher increase in the effective power. Finally, it can also be noted that the ratio $\%\Delta P_E / \%\Delta C_F$ is in the range of $65\% \div 70\%$, as would be expected (Schultz et al., 2011).

Table 9: Effective power variation $(\%\Delta P_E)$ of the full-scale KCS at 24 knots $(Fn = 0.26)$.

Test Surfaces	$\%\Delta P_{E_{CFD}}$
AF01	-2.05%
BL01	0.93%
FR01	0.23%
FR02	-3.56%
Sand 220	26.66%
Sand 60-80	36.12%

4 CONCLUSIONS AND FUTURE WORK

An experimental and CFD study was carried out to investigate the full ship hydrodynamic performance of different fouling control coatings and mimicked biofouling. The experimental part of the study led to the

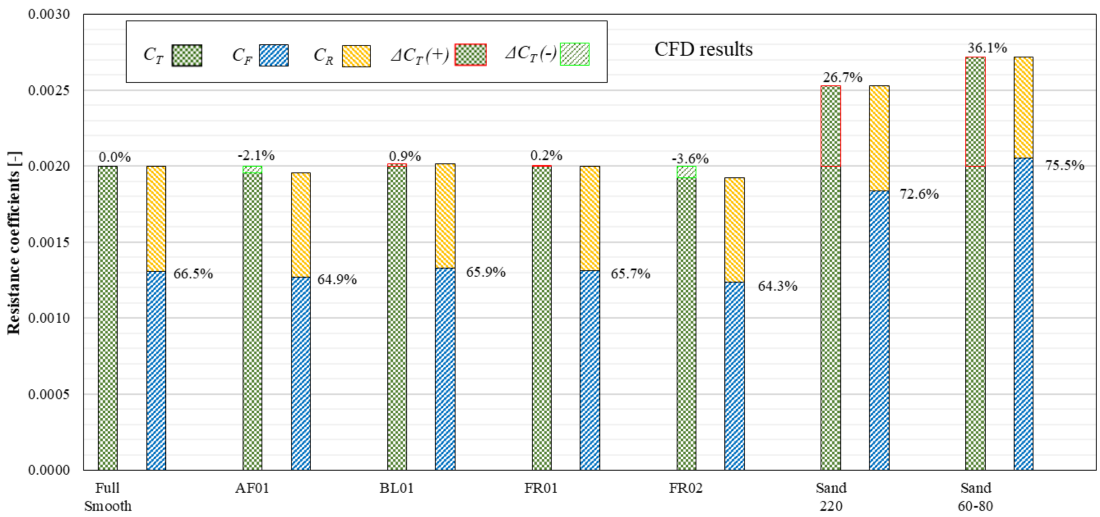

Figure 12: Percentage bar diagram of the resistance coefficients in different hull roughness.

introduction of novel experimental roughness functions for the FCCs tested including GIT's novel hard foul-release coating (*FR02*), while the numerical part scaled up the laboratory results to the size of a full ship length. The experimental roughness functions of the test surfaces were developed based on the pressure drop measurements conducted with the Fully Turbulent Flow Channel (FTFC) facility of the University of Strathclyde. The newly developed roughness functions of the fouling control coatings and sanded surfaces were implemented into the modified wall function approach in CFD using the Star-CCM+ software to provide scale-up results to ship length. The benchmark KRISO containership (KCS) hull in full-scale was chosen to calculate the variance of resistance and powering requirements due to different test surfaces at the design speed of 24 knots ($Fn = 0.26, Re = 2.72 \cdot 10^9$).

Among the four fouling control coatings (FCCs) that were tested in the FTFC, the *FR02* coating (hard foul-release) displayed the best hydrodynamic performance across the entire Reynolds number range. In fact, *FR02* displayed lower frictional resistance coefficients than if the ship was considered as smooth as the acrylic reference panel (5.57% decrease). Furthermore, *FR02* led to a maximum decrease in effective power requirements of 3.6%. The results of the numerical prediction also show that the *AF01* (self-polishing antifouling coating) have better hydrodynamic performance than the smooth reference case (maximum decrease in effective power requirements of 2.1%). In contrast, *Sand 220* (medium light slime) and *Sand 60-80* (medium slime) have, as expected, the highest resistance due to their rougher characteristics. In fact, a ship hull with medium light slime (*Sand 220*) and medium slime (*Sand 60-80*) surface roughness characteristics as the test surfaces would experience a maximum increase in effective power requirements of 26.7% and 36.1%, respectively.

Further investigation could be conducted on the prediction of resistance of the coatings at different speeds, on different hulls, and using heterogeneous patch distribution of the roughness. It will also be beneficial to investigate the hydrodynamic performance of the same fouling control coating under the effect of biofouling growth. Exposing surfaces to dynamically grown biofouling will give shipowners and operators a better indication of what powering penalty they should expect from these coatings after a certain time in active service. Finally, applying different mimicked biofouling to the panels before or after the coating application could also serve as a better method to predict the resistance behaviour of the as-applied condition to an existing rough ship hull.

Above all, the present study has provided several important findings, including the procedure to conduct pressure drop measurements with a FTFC, the application of Granville's method for pipes to develop roughness functions, as well as the introduction of roughness functions for novel or widely adopted marine surfaces and mimicked biofouling. The findings presented can help predict the required power, fuel consumption and greenhouse gas emissions of ships with hulls coated with certain fouling control coatings and/or in the fouled condition. As a final remark, the authors would like to emphasise that there is an enormous opportunity for growth around research on FTFCs. Indeed, the present study only represents an infinitesimal fraction of the number of coating products and surface roughness conditions that can be tested.

ACKNOWLEDGEMENTS

The research presented in this paper was carried out as a collaboration across the University of Strathclyde (https://www.strath.ac.uk/) and Dalhousie University (https://www.dal.ca/), with the support of Graphite Innovation and Technologies (https://www.grapheneenterprise.ca/). Furthermore, the authors gratefully acknowledge that the research presented in this paper was carried out as part of the EU funded H2020 project, VENTuRE (grant no. 856887, https://h2020venture.eu/), and the present work was also supported by Inha University Research Grant (http://eng.inha.ac.kr/). It should be noted that the results presented in this study were obtained using the ARCHIE-

WeSt High-Performance Computer (www.archie-west.ac.uk).

REFERENCES

Cebeci, T., Bradshaw, P., 1977. Momentum transfer in boundary layers. Washington, D.C., Hemisph. Publ. Corp.; New York, McGraw-Hill B. Co. 407.

Celik, I., Ghia, U., Roache, P., Freitas, C., Coleman, H., Raad, P., 2008. Procedure for Estimation and Reporting of Uncertainty Due to Discretization in CFD Applications. J. Fluids Eng. 130. https://doi.org/10.1115/1.2960953

Colebrook, C.F., Inst, A.M.C.E., Thomas, M., 1939. A New Theory of Turbulent Flow in Liquids of Small Viscosity. J. Inst. C.E 11, 611.

Coleman, H.W., Steele, W.G., 2012. Engineering application of experimental uncertainty analysis 33, 1888–1896. https://doi.org/10.2514/3.12742

Demirel, Y.K., 2015. Modelling the Roughness Effects of Marine Coatings and Biofouling on Ship Frictional Resistance. University of Strathclyde. https://doi.org/https://doi.org/10.48730/4b6n-9153

Demirel, Y.K., Uzun, D., Zhang, Y., Fang, H.-C., Day, A.H., Turan, O., 2017. Effect of barnacle fouling on ship resistance and powering. Biofouling 33, 819–834. https://doi.org/10.1080/08927014.2017.1373279

Dogrul, A., Song, S., Demirel, Y.K., 2020. Scale effect on ship resistance components and form factor. Ocean Eng. 209, 107428. https://doi.org/10.1016/j.oceaneng.2020.107428

Ferziger, J.H., Perić, M., Street, R.L., 2020. Computational Methods for Fluid Dynamics, Computational Methods for Fluid Dynamics. Springer International Publishing. https://doi.org/10.1007/978-3-319-99693-6

Granville, P.S., 1987. Three indirect methods for the drag characterization of arbitrarily rough surfaces on a flat plates. J. Sh. Res. 31, 70–77.

Granville, P.S., 1978. Similarity-law characterization methods for arbitrary hydrodynamic roughnesses. Bethesda: Rockville, MD, USA.

Granville, P.S., 1958. The Frictional Resistance and Turbulent Boundary Layer of Rough Surfaces. J. Sh. Res. 2, 52–74. https://doi.org/10.5957/jsr.1958.2.4.52

Grigson, C., 1992. Drag Losses of New Ships Caused by Hull Finish. J Sh. Res 36, 182.

ITTC, 2014. Executive Committee Final report and recommendations to the 27 th ITTC.

ITTC, 2011a. ITTC-Recommended Procedures-Fresh Water and Seawater Properties, in: 26th International Towing Tank Conference. Rio de Janeiro, pp. 1–45.

ITTC, 2011b. ITTC-Recommended Procedures and Guidelines Practical Guidelines for Ship CFD Applications.

KCS Geometry and Conditions [WWW Document], 2008. . SIMMAN 2008, FORCE Technol. URL http://www.simman2008.dk/KCS/kcs_geometry.htm

Kim, W.J., Van, S.H., Kim, D.H., 2001. Measurement of flows around modern commercial ship models. Exp. Fluids 31, 567–578. https://doi.org/10.1007/s003480100332

Larsson, L., Stern, F., Visonneau, M., 2013. CFD in ship hydrodynamics - Results of the Gothenburg 2010 workshop, in: Computational Methods in Applied Sciences. Springer Netherland, pp. 237–259. https://doi.org/10.1007/978-94-007-6143-8_14

Marino, A., Shi, W., Atlar, M., Demirel, Y.K., 2019. Design specification, commission and calibration of the University of Strathclyde's Fully Turbulent Flow Channel (FTFC) facility, in: 6th International Conference on Advanced Model Measurements Technologies for The Maritime Industry (AMT'19). Rome.

Nikuradse, J., 1933. Laws of flow in rough pipes, NACA Technical Memorandum, 1292.

Ravenna, R., 2019. Experimental Investigation on the Effect of Biomimetic Tubercles and Roughness on the Hydrodynamics of a Flat Plate. University of Strathclyde, Università degli studi di Trieste.

Ravenna, R., Marino, A., Song, S., Atlar, M., Turan, O., Day, S., Demirel, Y.K., 2022a. Experimental study on the effect of biomimetic tubercles on the drag of a flat plate. Ocean Eng. 255, 111445. https://doi.org/10.1016/J.OCEANENG.2022.111445

Ravenna, R., Marino, A., Song, S., Demirel, Y.K., Atlar, M., Turan, O., 2019. Experimental Investigation on the Effect of Biomimetic Tubercles on the Hydrodynamics of a Flat Plate. Int. J. Mech. Ind. Eng.

Ravenna, R., Song, S., Shi, W., Sant, T., De Marco Muscat-Fenech, C., Tezdogan, T., Demirel, Y.K., 2022b. CFD analysis of the effect of heterogeneous hull roughness on ship resistance. Ocean Eng. 258, 111733. https://doi.org/10.1016/J.OCEANENG.2022.111733

Richardson, L.F., 1911. IX. The approximate arithmetical solution by finite differences of physical problems involving differential equations, with an application to the stresses in a masonry dam. Philos. Trans. R. Soc. London. Ser. A, Contain. Pap. a Math. or Phys. Character 210, 307–357. https://doi.org/10.1098/RSTA.1911.0009

Schultz, M.P., 2007. Effects of coating roughness and biofouling on ship resistance and powering.

Biofouling 23, 331–341. https://doi.org/10.1080/08927010701461974

Schultz, M.P., 2004. Frictional resistance of antifouling coating systems. J. Fluids Eng. Trans. ASME 126, 1039–1047. https://doi.org/10.1115/1.1845552

Schultz, M.P., Bendick, J.A., Holm, E.R., Hertel, W.M., 2011. Economic impact of biofouling on a naval surface ship. Biofouling 27, 87–98. https://doi.org/10.1080/08927014.2010.542809

Schultz, M.P., Flack, K.A., 2007. The rough-wall turbulent boundary layer from the hydraulically smooth to the fully rough regime. J. Fluid Mech. 580, 381–405. https://doi.org/10.1017/S0022112007005502

Schultz, M.P., Walker, J.M., Steppe, C.N., Flack, K.A., 2015. Impact of diatomaceous biofilms on the frictional drag of fouling-release coatings. Biofouling 31, 759–773. https://doi.org/10.1080/08927014.2015.1108407

Siemens, 2020. STAR-CCM+, User Guide. Version 15.06.

Song, S., Dai, S., Demirel, Y.K., Atlar, M., Day, S., Turan, O., 2021a. Experimental and theoretical study of the effect of hull roughness on ship resistance. J. Sh. Res. 65, 62–71. https://doi.org/10.5957/JOSR.07190040

Song, S., Demirel, Y.K., Atlar, M., 2020a. Penalty of hull and propeller fouling on ship self-propulsion performance. Appl. Ocean Res. 94, 102006. https://doi.org/10.1016/j.apor.2019.102006

Song, S., Demirel, Y.K., Atlar, M., 2020b. Penalty of hull and propeller fouling on ship self-propulsion performance. Appl. Ocean Res. 94, 102006. https://doi.org/10.1016/j.apor.2019.102006

Song, S., Demirel, Y.K., Atlar, M., Dai, S., Day, S., Turan, O., 2020c. Validation of the CFD approach for modelling roughness effect on ship resistance. Ocean Eng. 200, 107029. https://doi.org/10.1016/j.oceaneng.2020.107029

Song, S., Demirel, Y.K., De Marco Muscat-Fenech, C., Sant, T., Villa, D., 2021b. Investigating the Effect of Heterogeneous Hull Roughness on Ship Resistance Using CFD. J. Mar. Sci. Eng. 9. https://doi.org/10.3390/jmse9020202

Song, S., Ravenna, R., Dai, S., De Marco Muscat-Fenech, C., Tani, G., Demirel, Y.K., Atlar, M., Day, S., Incecik, A., 2021c. Experimental investigation on the effect of heterogeneous hull roughness on ship resistance. Ocean Eng. 223. https://doi.org/10.1016/j.oceaneng.2021.108590

Tezdogan, T., Demirel, Y.K., Kellett, P., Khorasanchi, M., Incecik, A., Turan, O., 2015. Full-scale unsteady RANS CFD simulations of ship behaviour and performance in head seas due to slow steaming. Ocean Eng. 97, 186–206. https://doi.org/10.1016/j.oceaneng.2015.01.011

Yeginbayeva, I.A., Atlar, M., 2018. An experimental investigation into the surface and hydrodynamic characteristics of marine coatings with mimicked hull roughness ranges. Biofouling 34, 1001–1019. https://doi.org/10.1080/08927014.2018.1529760

Yeginbayeva, I.A., Atlar, M., Turkmen, S., Chen, H., 2020. Effects of 'in-service' conditions–mimicked hull roughness ranges and biofilms–on the surface and the hydrodynamic characteristics of foul-release type coatings. Biofouling 36, 1074–1089. https://doi.org/10.1080/08927014.2020.1855330